small
NANO MICRO

Watching Single Nanoparticles Grow in Real Time through Supercontinuum Spectroscopy

*Lars O. Herrmann and Jeremy J. Baumberg**

Over the past decade, gold nanorods (AuNRs) have evolved from a versatile research tool into a serious contender for commercial applications such as information storage,[1,2] integrated nanoscale optical devices,[3,4] and sensing.[5–8] The majority of these applications rely on precise assembly and growth of nanorod structures on surfaces. However controlled assembly and reproducible synthesis of AuNRs remains a major challenge which can only be addressed through a deeper understanding of the growth process. Unfortunately ensemble measurements such as extinction spectroscopy and X-ray scattering provide ambiguous results due to their inherent statistical nature.[9–17] On the other hand, conventional techniques capable of monitoring single particle growth such as atomic force microscopy and conventional dark-field (DF) spectroscopy do not provide sufficient time-resolution to extract precise quantitative information about the growth process.[18–21] In order to overcome this limitation, we use a supercontinuum laser to perform DF spectroscopy in a focused mode which enables acquisition of full broadband scattering spectra on a millisecond timescale in situ. This is over 100 times faster than can typically be achieved with a conventional DF spectroscopy setup. We use this technique to observe the growth of a single AuNR and to extract precise quantitative information about its growth kinetics.

Previous studies have reported interferometric techniques for millisecond detection of small particles such as viruses using conventional illumination sources,[22,23] as well as in combination with a white-light laser to record plasmon spectra of gold nanoparticles.[24] These techniques do not measure the pure scattering signal, but an interferometric signal which for small particles scales as d^3 (where d is the size of the nanoparticle) rather than d^6. This allows spectroscopic measurements of very small particles down to 5 nm diameter, even though the dependence of the signal on particle size follows a non-trivial trend. On the other hand, the setup presented here measures the pure scattering of nanoparticles, and for particles larger than ~50 nm achieves a similar performance to the interferometric method, since the scattering dominates the spectral response. A more recent study describes the use of white-light lasers for total internal reflection microscopy (TIR) to observe the deposition of proteins on an AuNR with millisecond time-resolution.[25] Due to the exponentially decaying field behind the refractive surface, this technique is limited to the immediate vicinity of surfaces.[23,26] The advantage of the DF illumination described here is the capability to probe deep into a sample (for instance in a fluid) which is crucial for many applications such as spectroscopic observation of optically trapped nanoparticles, bio-imaging and hyperspectral mapping of three dimensional nanostructures.[27,28] Moreover, it allows seamless integration into commercial microscopy systems.

To achieve the reported improvement in sensitivity and speed of DF spectroscopy, a coherent broadband white-light laser source (450–1700 nm) is employed. It is extremely bright (>1 W output power between 500–1000 nm) and can be focused to a near-diffraction limited spot, thereby confining illumination only to the region of interest. This enables tunable illumination intensities (radiant flux densities) to beyond 10 $MWcm^{-2}$ in the focal spot of the laser, whereas the light source of a conventional microscope only reaches of order 1 $kWcm^{-2}$. The combination of elevated brightness with a specular reflection background-free spectroscopic technique is responsible for the excellent signal-to-noise ratios (SNRs, ratios between signal peak and noise floor) achieved with the reported method.

In this setup (**Figure 1**a), the beam of a supercontinuum laser (Fianium SC450-6) is expanded and spatially filtered by a Keplerian beam expander (L1, P, L2), then passed through an absorptive ND1.3 and KG2 filter (F) to attenuate power and remove infrared radiation. A beam block (BB) removes the central part of the beam while the remaining ring-shaped beam travels through the outer part of a water immersion objective (Leica 63×, NA 1.2) and is focused through a coverslip to a near-diffraction limited spot. Both scattered and reflected light from the sample are collected by the objective, but only the light that is scattered into the central part of the objective through an iris (ID) can reach the spectrometer (OceanOptics QE65000) and CCD camera (Lumenera Infinity2-1RC). In addition to the coherent DF illumination, a halogen lamp in a Koehler configuration can be used for wide-field imaging in order to locate the sample. Scattering spectra of a gold nanosphere and a gold nanorod acquired

L. O. Herrmann, Prof. J. J. Baumberg
NanoPhotonics Centre
Cavendish Laboratory
University of Cambridge
Cambridge, CB3 0HE, UK
E-mail: jjb12@cam.ac.uk

DOI: 10.1002/smll.201300958

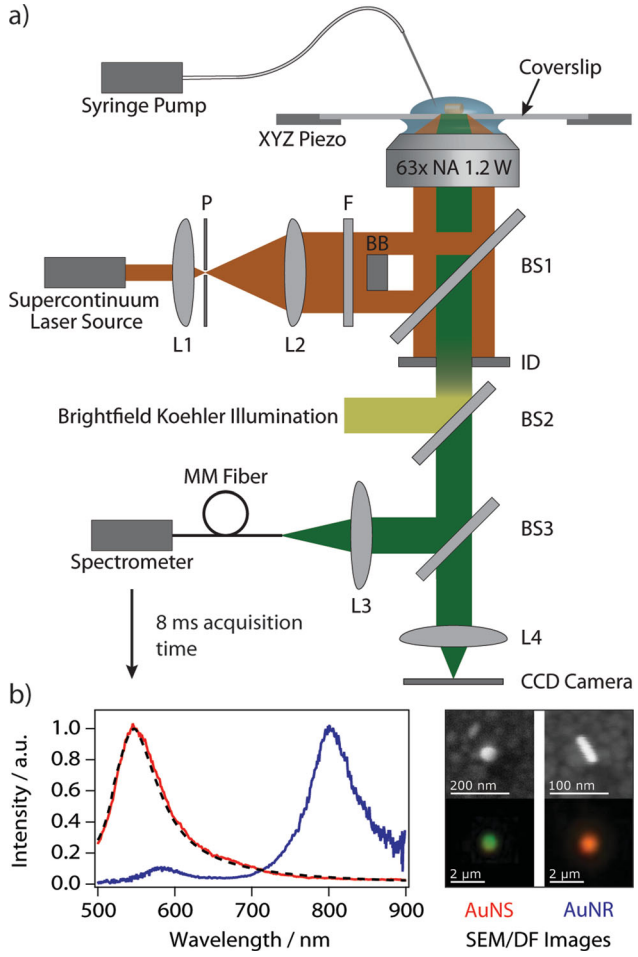

Figure 1. Inverted supercontinuum laser microscope setup for high-speed scattering spectroscopic measurements of gold nanoparticles in solution. a) Schematic of experimental setup. b) Normalized scattering spectra of 60 nm diameter gold nanosphere (AuNS, red), Mie theory (black dashed) and AuNR (blue). Spectra were acquired with an integration time of 8 ms. Correlated SEM and DF images are shown on the right.

in 8 ms show the high fidelity and SNR of this configuration (Figure 1b).

The growth of a single gold nanorod was monitored on an ITO-coated coverslip sparsely functionalized with rigidly anchored seed AuNRs. It was initiated by adding freshly-prepared growth solution and the process simultaneously monitored by supercontinuum laser DF spectroscopy (acquisition frequency 30 Hz, integration time 8 ms, average radiant flux density of illumination 75 kWcm^{-2}, see Supporting Information). After 70 seconds, the growth was stopped by rinsing the coverslip with deionized water. High-magnification scanning electron microsope (SEM) images before and after growth of the AuNR were also recorded.

Two distinct plasmon resonances are observed at 604 ± 2 nm and 716 ± 2 nm in the acquired scattering spectra (**Figure 2**a). These spectral bands correspond to transverse and longitudinal coherent electron oscillations inside the AuNR, respectively. During the growth process observed, the longitudinal plasmon resonance (LPR) red-shifts from 716 ± 2 nm to 829 ± 2 nm. This red-shift is accompanied by a broadening of the full width at half maximum (FWHM) of the resonance from 67 ± 3 nm to 90 ± 5 nm. At the same time, the transverse plasmon resonance (TPR) undergoes a slight blue-shift from 604 ± 2 nm to 590 ± 2 nm and thereby we observe the change in depolarization factor in real time as the rod lengthens.[11] Overall, the scattered intensity of the AuNR between 500 nm and 900 nm increases by 127% (Figure 2a inset). The observed intensity fluctuations are partly attributed to variations of the refractive index of the surrounding medium due to approaching molecules during the growth process, but also stem from output power fluctuations of the laser source (see Supporting Information). This is substantiated by the high correlation (r = 0.98, p-value 0.005) between the peak intensity changes of TPR and LPR. The SNR of the acquired spectra is estimated to be around 100 times larger than those achievable with a conventional dark-field microscope on a similarly sized AuNP (cf. Supporting Information).[18]

Furthermore, the correlated SEM images reveal a significant elongation of the AuNR from 87 ± 4 nm to 140 ± 4 nm, while its diameter stays approximately constant at 36 ± 4 nm (Figure 2b). This corresponds to a change in the aspect ratio (length/diameter) from 2.4 ± 0.3 to 3.9 ± 0.4, in good agreement with the change predicted from the LPR position based on Gans' theory.[12] Using a nearby defect on the ITO surface as reference point, it is found that the AuNR grew approximately 4 times faster at its left than at its right end. This indicates that the growth rate is very sensitive to local factors such as rod end surface morphology and capping layer density. The DF image turns from dark red to orange due to the fall-off in quantum efficiency of the CCD camera in the NIR region towards which the longitudinal mode is shifted.

It is well-established that the dominant gold-containing species present in the growth solution before the addition of ascorbic acid (AA) is $[Au^{3+}Br_4]^-$.[13,29–32] The bromide ions originate from partially dissociated hexadecyltrimethylammonium bromide (CTAB). Upon addition of AA, Au^{3+} is reduced in a two electron process to $[Au^{1+}Br_2]^-$ while AA is oxidized to dehydroascorbic acid (DA). Subsequently, DA partly decomposes into 2,3-diketo-1-gulonic acid via hydrolysis.[33] It is noteworthy that neither AA nor its oxidation products are able to reduce gold to its elemental form at room temperature.[34] On contact with growth solution, the exposed surface of AuNR (i.e. Au^0) is understood to catalyze the disproportionation of Au^{1+} to elemental Au^0 according to the equation:

$$3[Au^{1+}Br_2]^- \rightarrow 2Au^0 + [Au^{3+}Br_4]^- + 2Br^-$$

CTAB is known to bind preferentially to the sides of the rods rather than to the capping end crystal planes.[35] Therefore, over time more Au^0 atoms are exposed at the tips of the rod, which become available to participate in catalysis. This means that the rod is expected to grow much faster along its longitudinal axis. This phenomena is indeed observed in the acquired SEM images as well as the scattering spectra, as discussed earlier (Figure 2b).

small 2013,
DOI: 10.1002/smll.201300958

small NANO MICRO

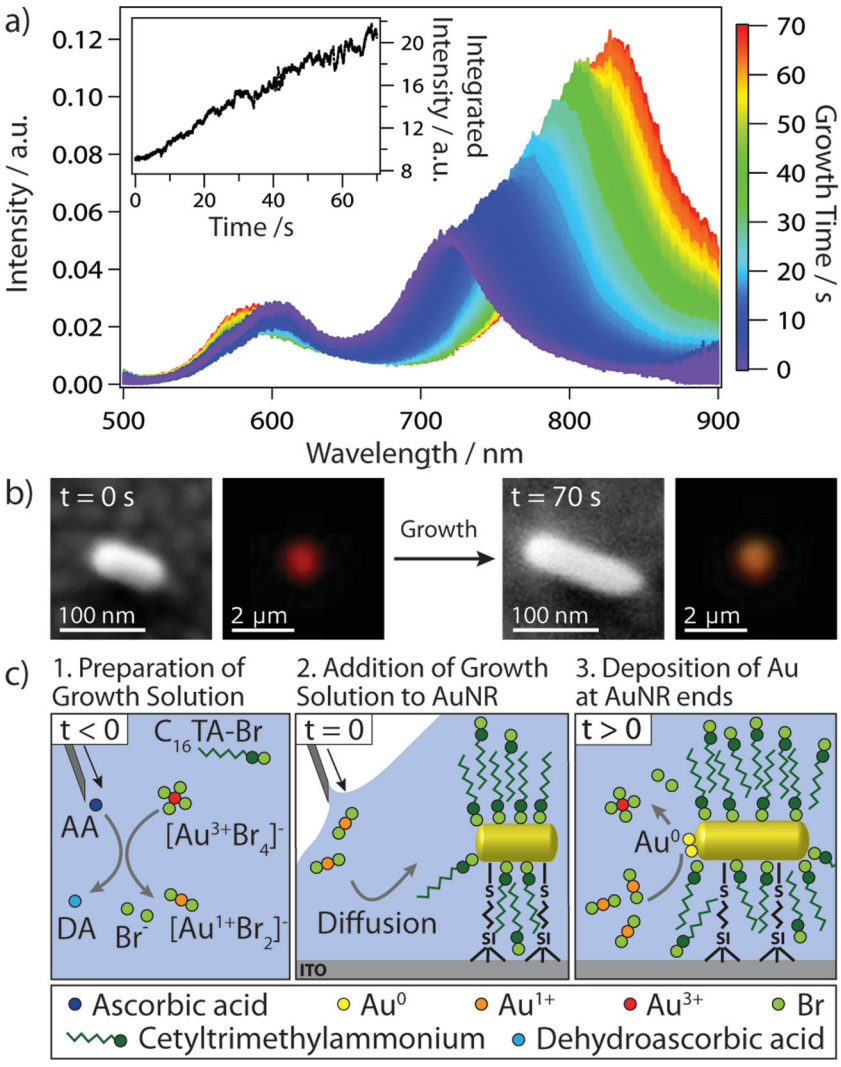

Figure 2. a) Scattering spectra of growing AuNR acquired at 30 Hz. The longitudinal plasmon resonance strongly red-shifts while the transverse resonance slightly blue-shifts. Inset shows change in integrated intensity over time. b) Correlated SEM and DF images of AuNR before and after growth. c) Schematic of AuNR growth via two step reduction of Au-ions (not drawn to scale). For simplicity, CTAB micelles are omitted.

To further the understanding of the growth kinetics on the time-scales of this study, the size information from correlated SEM images is used for finite-difference time-domain simulations (FDTD, Lumerical). From these simulations, the AuNR length can be determined from its LPR position as a function of time. Due to the negligible increase in rod diameter, it is assumed that the volume of the rod is proportional to its length. Based on this assumption, the time-dependent growth rate of the AuNR is calculated. The reduction rate initially sharply increases, reaches a maximum of 93 atoms/ms roughly 10 s after addition of the growth solution and then continually drops to an approximately constant 25 atoms/ms. In other words, the initially active rod facet area increases by 60% within the first 10 s and it is assumed that this is due to partial displacement of CTAB by the newly deposited Au atoms. The total number of atoms at the end of the rod is of order 10^4. Of these atoms ~1% react each millisecond to maintain the growth rate of ~100 atoms/ms. This corresponds to a molecular rate of 1 reaction per atom per 100 ms. The time evolution of the LPR and TPR of the AuNR and the extracted time-dependent length and growth rate shown in **Figure 3**a and b clearly demonstrate the capability to directly measure attogram deposition on millisecond timescales. The excellent SNR ratio enables precise fitting of the LPR position ($\sigma <$ 0.1 nm) and thereby allows resolution of the deposition of <1000 atoms. In other words, the deposition of single atomic layers on the rod end facets can be measured. Hence, the technique here provides the same resolution in determining the relative change in rod length as transmission electron microscopy, but directly in solution during growth in real time.

Based on the previously outlined accepted growth mechanism, the reduction of Au^{1+} to Au^0 which is an autocatalytic reaction is expected to occur in three phases. Phase I (induction period) is an initial phase of slow growth, because only a small amount of accessible surface facet Au^0 is present to catalyze the reduction. This is followed by phase II, where the growth rate progressively increases as the amount of gold deposited on the rod creates new facets, increasing the surface area. The growth of the rod continues until all available Au^{1+} is depleted in the close vicinity of the AuNR, resulting in a final plateau phase (Phase III). These kinetics are well described by a sigmoidal curve (Figure 3c, red dashed line).[36,37]

In this study, due to the presence of a preformed AuNR, the very first stage of extremely slow initial autocatalytic growth (phase I) is partially bypassed. However, the amount of reduced gold after addition of growth solution accurately follows phase II (green line in Figure 3c). After approximately 10 s, depletion of Au^{1+} in the vicinity of the AuNR starts to slow down the deposition. In solution phase experiments, due to the sheer number of nucleation sites across many nanoparticles, this usually results in complete depletion of the reactants in the solution and the reaction stops. On the other hand, in surface studies all the nucleation sites are restricted to the AuNRs on the substrate, which means the Au^{1+} far away from the surface does not get depleted. From SEM images of the tethered seed AuNRs, the total number of reduced Au^0 atoms on the surface during the growth process was estimated to be on average 0.1 nm^{-2}, with over 10^3 nm^{-2} Au^{1+} available in solution. Thus, the solution phase effectively acts as an Au^{1+} reservoir, which constantly provides new ions that diffuse close to the AuNR ends where they are reduced. Consequently, a diffusion-limited growth rate is observed during phase III, rather than cessation of growth.

DOI: 10.1002/smll.201300958

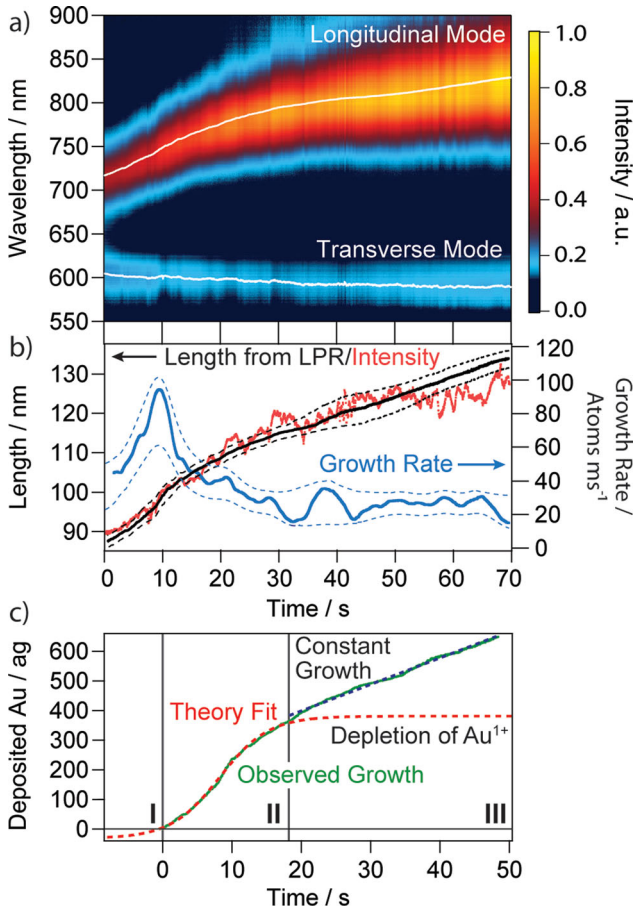

Figure 3. a) DF scattering spectra of growing AuNR as a function of time. As the aspect ratio of the AuNR increases its LPR redshifts and its TPR slightly blueshifts. b) Length (black from LPR, red from peak intensity) and gold deposition rate (blue) extracted from combination with FDTD simulations. The dashed lines show the limits set by the FWHM of the spectral lines and the error of the FDTD calculations. c) Amount of deposited Au (in attograms, solid green line) initially follows a sigmoidal curve (red, dashed) which indicates autocatalytic growth. Constant influx of Au^{1+} ions from bulk then leads to a diffusion-limited constant growth rate (blue dashed).

A qualitative model for this diffusion process can be derived from the steady state net flow J of Au^{1+} ions from a semi-infinite bath at concentration c_∞ to a hemispherical sink with radius r at the origin, given by[38] $J = 2\pi r D c_\infty$. From Figure 3b we know that the steady state flux to each rod end is $J = 1.25 \cdot 10^4\ s^{-1}$. With a hemispherical radius of $r = 18$ nm (based on the rod diameter obtained from the SEM images and the assumption that all Au atoms are accessible) and the known Au^{1+} concentration $c_\infty = 0.6$ mM, the diffusion constant of single Au^{1+} ions is estimated to be $D = 3 \cdot 10^{-13}\ m^2 s^{-1}$. The hydrodynamic radius of the diffusing species predicted by the Einstein-Stokes equation is thus of order 100 nm. This is three orders of magnitude larger than the radius of Au^{1+} and indicates that the Au^{1+} ions are bound to a much larger diffusing species. It has been proposed that these species are CTAB micelles (radius ~ 10 nm).[10,39] One reason our calculation may overestimate the size of these micelles is due to the assumption that all Au atoms at the rod end are exposed. This is clearly not the case, since CTAB limits the number of accessible atoms. On the other hand, this result implies that the magnitude of the ion flux to the rod ends can be explained solely by diffusion and no significant convection occurs. Strong laser induced heating during the growth process is thus unlikely to be relevant on these nm length-scales.

In conclusion, we have developed a widely-applicable and high-speed DF scattering spectroscopic technique. The ability to monitor plasmon resonances in situ on a millisecond timescale makes this an ideal tool to investigate nanoparticle synthesis in real time and other dynamic processes such as molecular switching or sensing applications. This is demonstrated through the real time in situ observation of growth of a single AuNR. Correlated SEM images in combination with FDTD simulations are employed to extract the time evolution of the length and growth rate of the AuNR. The observed deposition rate substantiates the proposed autocatalytic growth mechanism and provides detailed insight into growth kinetics obtained from single particle measurements. In addition, the excellent SNR of this technique opens up the possibility to resolve deposition of ~1000 atoms and therefore to measure relative weight changes of AuNPs with sub-attogram resolution. While we report measurements of a single AuNR here to demonstrate the power of this technique, ongoing work examines the diversity of different dynamics from different nanoparticle seeds.

Furthermore, our technique opens up exciting perspectives such as optochemical control of nanoparticle growth with real time feedback, monitoring single molecule catalytic reactions on gold nanocrystal surfaces or fast broadband hyperspectral imaging.

Experimental Section

Solutions and Chemicals: Hexadecyltrimethylammonium bromide (CTAB, 98%), silver nitrate (99%), gold(III) chloride hydrate (99.999%) and 3-mercaptopropyltrimethoxysilane (MPTMS, 95%) were purchased from Sigma-Aldrich (UK).

AuNR Synthesis and Growth: AuNRs were synthesized according to a previously reported protocol[40] which allows synthesis of short and relatively thick AuNRs (low aspect ratio). The growth of AuNRs attached to the surface was initiated through addition of 50 µL of a growth solution containing CTAB (0.1 M), $HAuCl_4$ (0.6 mM) and AA (1 mM).[41]

AuNR Surface Functionalization: ITO-coated coverslips with a surface resistivity of 15–30 Ω were purchased from SPI Supplies, USA. They were sonicated in acetone and 2-propanol for 15 min each, then functionalized by immersion in a MPTMS ethanol solution (5%) for 24 h. The coverslips were rinsed with deionized water and dried with nitrogen. A drop of AuNRs (100 µL) was placed on top of the coverslips and washed off with deionized water after 2 h. This resulted in very clean substrates with sparsely attached and well-separated AuNRs.

SEM/DF Spectroscopy Correlation: To aid comparison of electron microscopy and optical tracking, a focused ion beam (FIB) mark was milled into the surface of an ITO-coated coverslip with a Zeiss 1540XB CrossBeam workstation. This mark was then used as a proximity tag to select and identify an AuNR of interest (see Figure S3 in supporting information). The ion beam mark was

small 2013,
DOI: 10.1002/smll.201300958

NANO MICRO small

located using the bright-field Koehler illumination to place the previously selected AuNR in the center of the focal spot of the supercontinuum laser. The Zeiss CrossBeam workstation was also used to record all SEM images.

Supporting Information

Supporting Information is available from the Wiley Online Library or from the author.

Acknowledgements

The authors acknowledge funding from UK EPSRC grants EP/H028757/1, EP/H007024/1, EP/G060649/1, EU CUBIHOLES and ERC 320503 LINASS for this work. We also thank Setu Kasera, Sam Jones, Roger Coulston, and Oren Scherman for helpful discussions.

[1] J. W. M. Chon, C. Bullen, P. Zijlstra, M. Gu, *Adv. Funct. Mater.* **2007**, *17*, 875–880.
[2] P. Zijlstra, J. W. M. Chon, M. Gu, *Nature* **2009**, *459*, 410–413.
[3] A. M. Funston, C. Novo, T. J. Davis, P. Mulvaney, *Nano Lett.* **2009**, *9*, 1651–1658.
[4] D. K. Gramotnev, S. I. Bozhevolnyi, *Nature Photon.* **2010**, *4*, 83–91.
[5] C. Sönnichsen, A. P. Alivisatos, *Nano Lett.* **2005**, *5*, 301–304.
[6] C. J. Murphy, A. M. Gole, S. E. Hunyadi, J. W. Stone, P. N. Sisco, A. Alkilany, B. E. Kinard, P. Hankins, *Chem. Commun.* **2008**, *5*, 544–557.
[7] K. D. Alexander, K. Skinner, S. Zhang, H. Wei, R. Lopez, *Nano Lett.* **2010**, *10*, 4488–4493.
[8] L. Xu, H. Kuang, L. Wang, C. Xu, *J. Mater. Chem.* **2011**, *21*, 16759–16782.
[9] B. Nikoobakht, M. A. El-Sayed, *Chem. Mater.* **2003**, *15*, 1957–1962.
[10] J. Pérez-Juste, L. M. Liz-Marzán, S. Carnie, D. Y. C. Chan, P. Mulvaney, *Adv. Funct. Mater.* **2004**, *14*, 571–579.
[11] J. Pérez-Juste, I. Pastoriza-Santos, L. M. Liz-Marzán, P. Mulvaney, *Coord. Chem. Rev.* **2005**, *249*, 1870–1901.
[12] A. Gulati, H. Liao, J. H. Hafner, *J. Phys. Chem. B* **2006**, *110*, 22323–22327.
[13] J. a Edgar, A. M. McDonagh, M. B. Cortie, *ACS Nano* **2012**, *6*, 1116–1125.
[14] D. A. Zweifel, A. Wei, *Chem. Mater.* **2005**, *17*, 4256–4261.
[15] Y. Takenaka, H. Kitahata, *Phys. Rev. E* **2009**, *80*, 1–4.
[16] B. Abécassis, F. Testard, O. Spalla, P. Barboux, *Nano Lett.* **2007**, *7*, 1723–1727.
[17] A. Henkel, O. Schubert, A. Plech, C. Sönnichsen, *J. Phys. Chem. C* **2009**, *113*, 10390–10394.
[18] C. Novo, A. M. Funston, P. Mulvaney, *Nat. Nanotechnol.* **2008**, *3*, 598–602.
[19] J. Becker, O. Schubert, C. Sönnichsen, *Nano Lett.* **2007**, *7*, 1664–1669.
[20] Z. Wei, F. P. Zamborini, *Langmuir* **2004**, *20*, 11301–11304.
[21] Z. Wei, H. Qi, M. Li, B. Tang, Z. Zhang, R. Han, J. Wang, Y. Zhao, *Small* **2012**, *8*, 1331–1335.
[22] F. Ignatovich, L. Novotny, *Phys. Rev. Lett.* **2006**, *96*, 013901.
[23] J. Ortega-Arroyo, P. Kukura, *Phys. Chem. Chem. Phys.* **2012**, *9076*, 15625–15636.
[24] K. Lindfors, T. Kalkbrenner, P. Stoller, V. Sandoghdar, *Phys. Rev. Lett.* **2004**, *93*, 3–6.
[25] I. Ament, J. Prasad, A. Henkel, S. Schmachtel, C. Sönnichsen, *Nano Lett.* **2012**, *12*, 1092–1095.
[26] C. Sönnichsen, S. Geier, N. E. Hecker, G. von Plessen, J. Feldmann, H. Ditlbacher, B. Lamprecht, J. R. Krenn, F. R. Aussenegg, V. Z.-H. Chan, J. P. Spatz, M. Möller, *Appl. Phys. Lett.* **2000**, *77*, 2949–2951.
[27] W. Ni, H. Ba, A. a Lutich, F. Jäckel, J. Feldmann, *Nano Lett.* **2012**, *12*, 4647–4650.
[28] I. Itzkan, L. Qiu, H. Fang, M. M. Zaman, E. Vitkin, I. C. Ghiran, S. Salahuddin, M. Modell, C. Andersson, L. M. Kimerer, P. B. Cipolloni, K.-H. Lim, S. D. Freedman, I. Bigio, B. P. Sachs, E. B. Hanlon, L. T. Perelman, *Proc. Natl. Acad. Sci. USA* **2007**, *104*, 17255–17260.
[29] H. M. Chen, R. S. Liu, K. Asakura, L. Y. Jang, J. F. Lee, *J. Phys. Chem. B* **2007**, *111*, 18550–18557.
[30] L. G. Abdelmoti, F. P. Zamborini, *Langmuir* **2010**, *26*, 13511–13521.
[31] Y. Niidome, Y. Nakamura, K. Honda, Y. Akiyama, K. Nishioka, H. Kawasaki, N. Nakashima, *Chem. Commun.* **2009**, 1754–1756.
[32] T. Placido, R. Comparelli, F. Giannici, P. D. Cozzoli, G. Capitani, M. Striccoli, A. Agostiano, M. L. Curri, *Chem. Mater.* **2009**, *21*, 4192–4202.
[33] A. Bode, L. Cunningham, R. Rose, *Clin. Chem.* **1990**, *36*, 1989–1991.
[34] L. Gou, C. Murphy, *Chem. Mater.* **2005**, *26*, 9370–9374.
[35] C. J. Murphy, L. B. Thompson, D. J. Chernak, J. A. Yang, S. T. Sivapalan, S. P. Boulos, J. Huang, A. M. Alkilany, P. N. Sisco, *Curr. Opin. Colloid Interface Sci.* **2011**, *16*, 128–134.
[36] M. A. Watzky, R. G. Finke, *J. Am. Chem. Soc.* **1997**, *119*, 10382–10400.
[37] N. Jana, L. Gearheart, C. Murphy, *Chem. Mater.* **2001**, *13*, 2313–2322.
[38] R. Senthamarai, L. Rajendran, *Electrochim. Acta* **2008**, *53*, 3566–3578.
[39] P. Goyal, B. Dasannacharya, *Physica B* **1991**, *174*, 196–199.
[40] T. K. Sau, C. J. Murphy, *Langmuir* **2004**, *20*, 6414–6420.
[41] Z. Wei, A. J. Mieszawska, F. P. Zamborini, *Langmuir* **2004**, *20*, 4322–4326.

Received: March 26, 2013
Published online: